photonics

Article

Improved Sensitivity of Brain Cancer Detection Using 2D Photonic Crystal Sensor

Sarra Bendib [1,2], Nadhir Djeffal [3,4], Abderrahim Yousfi [1,2], Okba Saidani [1,2] and Abdallah Hedir [5,6,*]

[1] IET Institute, University of Mohamed Elbachir Elibrahimi, Al Anasser, Bordj Bou Arreridj 34030, Algeria; sarra.bendib@univ-bba.dz (S.B.); abderrahim.yousfi@univ-bba.dz (A.Y.); okba.saidani@univ-bba.dz (O.S.)
[2] MMN Team of ETA Laboratory, University of Mohamed Elbachir Elibrahimi, Bordj Bou Arreridj 34030, Algeria
[3] Faculty of Electrical Engineering and Computer Science, University of Mouloud MAMMERI, Tizi Ouzou 15000, Algeria; nadhir.djeffal@ummto.dz
[4] ETA Laboratory, University of Mohamed Elbachir Elibrahimi, Al Anasser, Bordj Bou Arreridj 34030, Algeria
[5] Laboratoire des Technologies Avancées en Génie Electrique (LATAGE), University of Mouloud MAMMERI, Tizi Ouzou 15000, Algeria
[6] Advanced High Voltage Engineering Centre, School of Engineering, Cardiff University, Queen's Buildings, The Parade, Cardiff CF24 3AA, UK
* Correspondence: abdallah.hedir@ummto.dz or hedira1@cardiff.ac.uk

Abstract

This study investigates the influence of cavity configuration on the performance of two-dimensional (2D) photonic crystal (PhC) sensors, with particular emphasis on the effect of doubling the number of cavities. A comparative analysis between single-cavity and dual-cavity configurations is conducted to evaluate their impact on key sensing parameters. In the dual-cavity configuration, two resonant cavities are introduced between coupled waveguides, enabling strong optical mode coupling and enhanced electromagnetic field confinement within the sensing region. This coupling leads to sharper resonance peaks, reduced linewidths, and increased interaction between the optical field and the infiltrated analyte. As a result, the dual-cavity sensor exhibits significantly improved sensing performance, achieving a high sensitivity of 9261.54 nm/RIU, a quality factor of 15,352.38, a figure of merit exceeding 4.5×10^7, and a detection limit below 1.7×10^{-7} RIU. These results demonstrate that doubling the cavity number effectively amplifies light–matter interaction and resonance stability, making the proposed dual-cavity 2D PhC sensor a highly promising platform for precise refractive index sensing in biomedical applications.

Keywords: photonic crystal; brain cancer; cavity; doubling cavity; optiFDTD

Received: 21 December 2025
Revised: 22 January 2026
Accepted: 10 February 2026
Published: 22 February 2026

1. Introduction

Early detection of cancer, particularly brain tumors, is critical due to the high mortality linked to late diagnoses. Traditional methods are expensive and complex, especially for brain imaging. Recently, photonic biosensors have emerged as powerful tools for label-free, rapid, and accurate cancer detection by sensing subtle changes in the refractive index (RI) of biological tissues [1]. This capability arises from a fundamental property of photonic crystals—the photonic band gap (PBG)—which prohibits light propagation within a specific frequency range. When defects are introduced into the periodic structure, its symmetry is broken, enabling strong electromagnetic field confinement. This leads to a longer photon lifetime, which enhances the interaction between light and matter. A higher quality factor

https://doi.org/10.3390/photonics13020207

results in a narrower resonance linewidth, directly improving the system's ability to detect smaller resonance shifts [2,3].

Recent research highlights the effectiveness of two-dimensional photonic crystal biosensors for detecting disease-related changes in biological samples by tracking refractive index variations. A dengue-focused design demonstrated high-quality resonance and strong sensitivity for identifying alterations in blood components [4]. Another study employed an annular photonic crystal structure operating in the terahertz range to correlate photonic band-gap shifts with refractive-index changes, achieving enhanced sensitivity through optimized ring-hole geometries [5]. Additionally, a malaria-oriented sensor exploited the differences between healthy and infected red blood cells, with grating-enhanced waveguides improving refractive-index detection accuracy [6]. Together, these studies emphasize the diagnostic potential of photonic crystal-based biosensing technologies.

To broaden the functionality of photonic crystal-based sensors, several studies have investigated the integration of functional materials that enable active tuning of optical properties under external stimuli. Magnetic-fluid-based photonic crystals, for example, have demonstrated tunable optical responses under applied magnetic fields and temperature variations. It has been reported that infiltrating magnetic fluids into resonant cavities can significantly enhance sensor sensitivity and performance [7]. Other studies have shown that temperature variations mainly affect the number of photonic band gaps, while their central frequencies remain relatively stable [8]. Additionally, in one-dimensional photonic crystals, both the positions and widths of photonic band gaps have been effectively tuned using external magnetic fields [9]. Photonic crystal sensing platforms have also been widely explored for chemical, thermal, and magnetic sensing applications, demonstrating high sensitivity and tunability [10].

Building on these advances in disease-oriented photonic biosensing, recent investigations have expanded the application of photonic crystal architectures to neurological diagnostics, particularly in the detection of brain abnormalities. Although earlier studies primarily focused on refractive-index variations in blood constituents and pathogen-infected cells, these same optical principles can be effectively extended to the subtle refractive-index contrasts present in brain tissues. This progression opens the pathway toward highly sensitive, label-free, and non-invasive photonic techniques for improving early detection and characterization of neurological disorders.

Recent advancements in photonic biosensing have highlighted the potential of photonic crystal (PhC) structures in non-invasive and label-free detection of brain abnormalities. One-dimensional (1D) PhCs have been widely explored for their high sensitivity and sharp defect modes. Walaa M. Nouman demonstrated the theoretical detection of brain lesions using a 1D defected photonic crystal analyzed via the Transfer Matrix Method (TMM), achieving a remarkable sensitivity of 3080.81 nm/RIU and a high figure of merit (FOM = 6.1×10^7 1/RIU) by observing the redshift in resonant wavelength corresponding to variations in the refractive index of brain tissues [11].

In parallel, Manal A. Maher et al. explored the thermal sensing capabilities of a 1D PhC sensor comprising layers of gallium nitride, glycerin, and air. Through TMM-based modeling in MATLAB, they optimized the sensor for temperature sensitivity ($\approx$10 nm/°C) and achieved a quality factor as high as 35,443, highlighting the impact of thermo-optic effects and defect layer thickness on sensing performance [12].

Furthermore, C. Malek introduced thermal and angular tunability via a nanocomposite superconducting layer, pushing sensitivity to 4139.24 nm/RIU [1]. These studies highlight the potential of 1D PhCs for accurate and tunable brain tissue sensing. In 2D PhCs Walaa M. Nouman achieved a sensitivity of 3080.81 nm/RIU and a figure of merit (FOM) of 6.1×10 using a defect-based 2D PhC sensor for brain lesion detection [11]. Meanwhile, other studies have introduced thermal and structural tunability to enhance sensor performance, reaching quality factors exceeding 35,000. However, Nazmi Achraf presented a compact 2D PhC sensor capable of differentiating between normal and malignant brain tissues with ultra-high quality factor (16,254) and a low detection limit of 9.08 × 10 [13]. Similarly, Sangeetha B. S. demonstrated that even slight variations in refractive index from 1.3333 to 1.4833 RIU can induce detectable shifts in a 2D PhC structure, achieving a quality factor of 283.72 [14]. Mohammed Boulesbaa further emphasized the dual-sensitivity response in both wavelength and intensity using a dual-cavity 2D PhC, attaining a sensitivity of 79.03 nm/RIU in wavelength and 285.44 [15]. Together, these contributions illustrate the rapid advancement of 1D and 2D photonic crystal biosensors, showcasing their potential for non-invasive, high-performance brain lesion detection through refractive index sensing and spectral shift analysis. This study presents a comparative investigation of how cavity number influences the performance of two-dimensional photonic crystal sensor designs for detecting brain lesions via cerebrospinal fluid refractive index analysis using OptiFTDT from the Optiwave (Version 12.1) package.

The structure of the paper is as follows. Section 2 describes in detail the structural design of the proposed device, including the signal-guiding mechanism and the dual-cavity configuration. Section 3 presents the photonic bandgap range of the structure. Section 4 discusses the sensing and detection mechanism, providing a comprehensive analysis of resonance wavelength shifts resulting from variations in the optical properties of different brain tissues. The device performance is evaluated for multiple brain cancer subtypes, including glioblastoma, medulloblastoma, lymphoma, and low-grade glioma, demonstrating high sensitivity and accurate subtype discrimination. Finally, Section 5 highlights the main conclusions of the study.

2. Structure and Design

This study explores two distinct two-dimensional (2D) photonic crystal (PhC) sensor architectures, each consisting of cylindrical GaAs rods of 3.5 refractive index distributed in air wafer with a respected lattice constant of 0.65 µm and integrating coupled waveguides with varying cavity configurations to enhance light–matter interactions for sensing applications.

Figure 1 represents the normal brain cells detection with two configurations: dual cavity and single cavity.

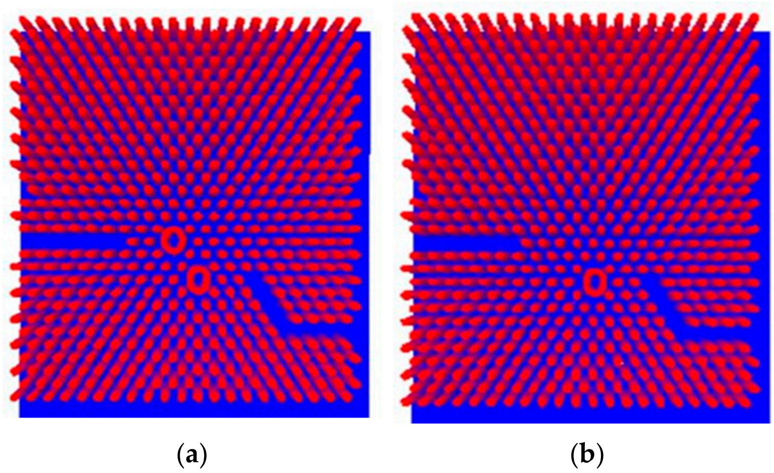
(**a**) (**b**)

Figure 1. Schematic of the proposed two-dimensional photonic crystal sensor structures: (**a**) dual-cavity configuration with coupled waveguides, and (**b**) single-cavity configuration with coupled waveguides. In both figures, the red color represents GaAs rods distributed in an air background.

- Single-Cavity Configuration:

The first structure features a single H0-type micro-cavity positioned between two intersecting photonic crystal waveguides forming a coupling region.

This cavity is formed by removing pillars within the PhC lattice, specifically by introducing an annular elliptical pillar at the center that has a major and minor radius of 500 and 350 nm, respectively, oriented at 90°.

- Dual-Cavity Configuration:

The second structure incorporates two adjacent H0-type micro-cavities between the coupled waveguides.

Each cavity is centered by an annular elliptical pillar with the same dimension as the first case. Figure 1 represents the proposed designs.

3. Band Gap Calculation

The band gap calculation has been affected using the Plane Wave Expansion (PWE) method, which is a computational technique used to calculate the band structure of photonic crystals. This method transforms Maxwell's equations into an eigenvalue problem by expanding both the electromagnetic fields and the dielectric function into Fourier series. Solving this eigenvalue problem yields the allowed electromagnetic modes and their corresponding frequencies, enabling the determination of photonic band gaps, which are frequency ranges where light propagation is forbidden.

In Figure 2 the photonic band gap is represented. The horizontal axis denotes the wave vectors Kx in units of $2\pi/a$, while the vertical axis indicates the normalized frequency in units of $\omega a/2\pi c$. Here, ω is the angular frequency of the incident microwave and c is the speed of light in vacuum. For TE polarization, a photonic band gap (PBG) is observed within the normalized frequency range of 0.65–0.71 ($\omega a/2\pi c$).

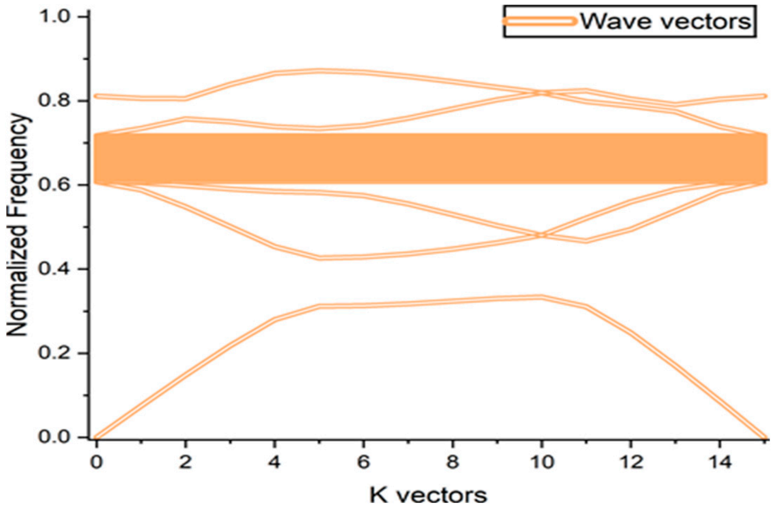

Figure 2. Photonic band gap of the proposed 2D PhC structure for TE polarization.

4. Detection Mechanism

Cerebrospinal fluid (CSF) is a clear, colorless liquid that surrounds the brain and spinal cord and plays a vital role in protecting and maintaining the central nervous system (CNS). It cushions neural tissues from mechanical shocks, delivers essential nutrients, removes metabolic waste, and helps regulate intracranial pressure [16].

In healthy individuals, the CSF has a refractive index (RI) of approximately 1.3333 in the infrared region. However, pathological conditions such as brain lesions or tumors can alter the composition of the CSF, leading to changes in its RI. Table 1 summarizes the refractive index of normal and malignant brain tissues.

Table 1. Refractive index values of normal and malignant brain tissues.

	Tissue	Refractive Index (RI)
Normal Cells	Cerebrospinal Fluid (CSF)	1.3333
	Wall of Brain	1.3412
	Multisclerosis	1.3425
	Oligodendroglioma	1.3353
	Gray Matter	1.3951
Malignant Cells	Medulloblastoma	1.4412
	White Matter	1.4121
	Low-Grade Glioma	1.4320
	Glioblastoma	1.4470
	Lymphoma	1.4591

There are different ways to obtain a sample of CSF. Lumbar puncture (spinal tap) is the most common method [17].

Figure 3 represents the detection mechanism where our structures are designed to allow infiltration of this CSF sample. When the analyte fills these regions, it changes the RI within the sensor. This alteration affects the propagation of light through the PhC, resulting in shifts in resonance wavelengths in the transmission spectrum.

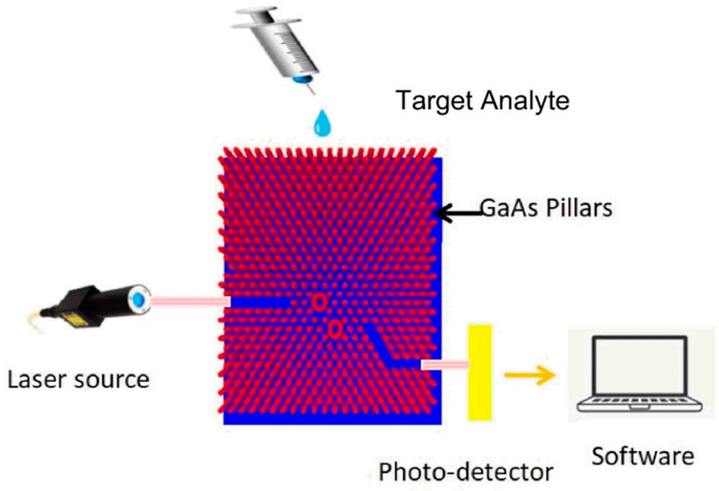

Figure 3. Structure and detection mechanism.

We perform wavelength sensitivity by quantifying the shift in the resonant wavelength per unit change in the refractive index of the analyte. It is defined by the following equation:

$$S_\lambda = \frac{\Delta\lambda}{\Delta n} \tag{1}$$

where

S_λ is the wavelength sensitivity;

λ_λ is the displacement of the transmission spectrum;

Δn is the RI change.

Following the sensitivity analysis, the single-cavity structure achieved a sensitivity of 200 nm/RIU, whereas the dual-cavity configuration reached 2888.61 nm/RIU. Given the enhanced sensitivity and performance demonstrated by the dual-cavity configuration, this design will be the main focus of subsequent analysis.

From a practical perspective, cerebrospinal fluid (CSF) samples obtained via lumbar puncture require only microliter scale volumes for refractive index-based optical sensing. In a practical implementation, the CSF can be introduced into the photonic crystal sensing region through microfluidic integration, enabling controlled infiltration into the cavity and waveguide regions. Standard preprocessing steps such as filtration or centrifugation may be applied to reduce the influence of cells and large biomolecules. The present work focuses on the intrinsic refractive index sensing mechanism under controlled conditions, while the influence of biological complexity is left for future experimental investigations.

To investigate the influence of cavity geometry on the sensing performance of the dual-cavity photonic crystal sensor under analyte infiltration, the inner radius of the annular cavities filled with water (serving as the reference analyte) was systematically varied from 400 nm to 375 nm and 350 nm, while all other structural parameters were kept unchanged. As shown in Figure 4, reducing the inner radius leads to noticeable modifications in the resonance wavelength position, peak intensity, and linewidth of the transmission spectrum. Smaller cavity dimensions enhance electromagnetic field confinement within the water-infiltrated sensing region, resulting in sharper resonance peaks and improved refractive index sensitivity. However, excessive size reduction introduces additional minor resonances and spectral distortions, indicating increased mode interaction and reduced spectral stability. These results confirm the existence of an optimal cavity geometry that balances strong field confinement with resonance robustness. Accordingly, an inner radius of 350 nm is adopted for all subsequent simulations to ensure optimal sensing performance.

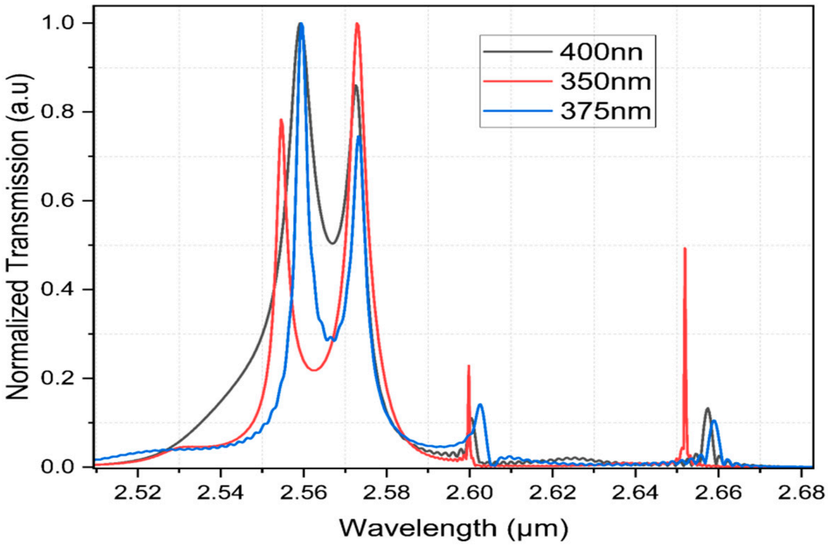

Figure 4. Effect of inner cavity radius variation (400 nm, 375 nm, and 350 nm) on the normalized transmission spectra of the dual-cavity photonic crystal sensor.

5. Results and Discussion

Figure 5a,b represent the normalized transmission detected at the output of single and dual-cavity structures using a spectrometer.

Figures 6 and 7 present three spectrally distinct resonant modes embedded within the photonic bandgap. The first mode manifests as a broad Gaussian-like spectral feature, characteristic of a low-Q resonance resulting from significant out-of-plane radiation and reduced field confinement.

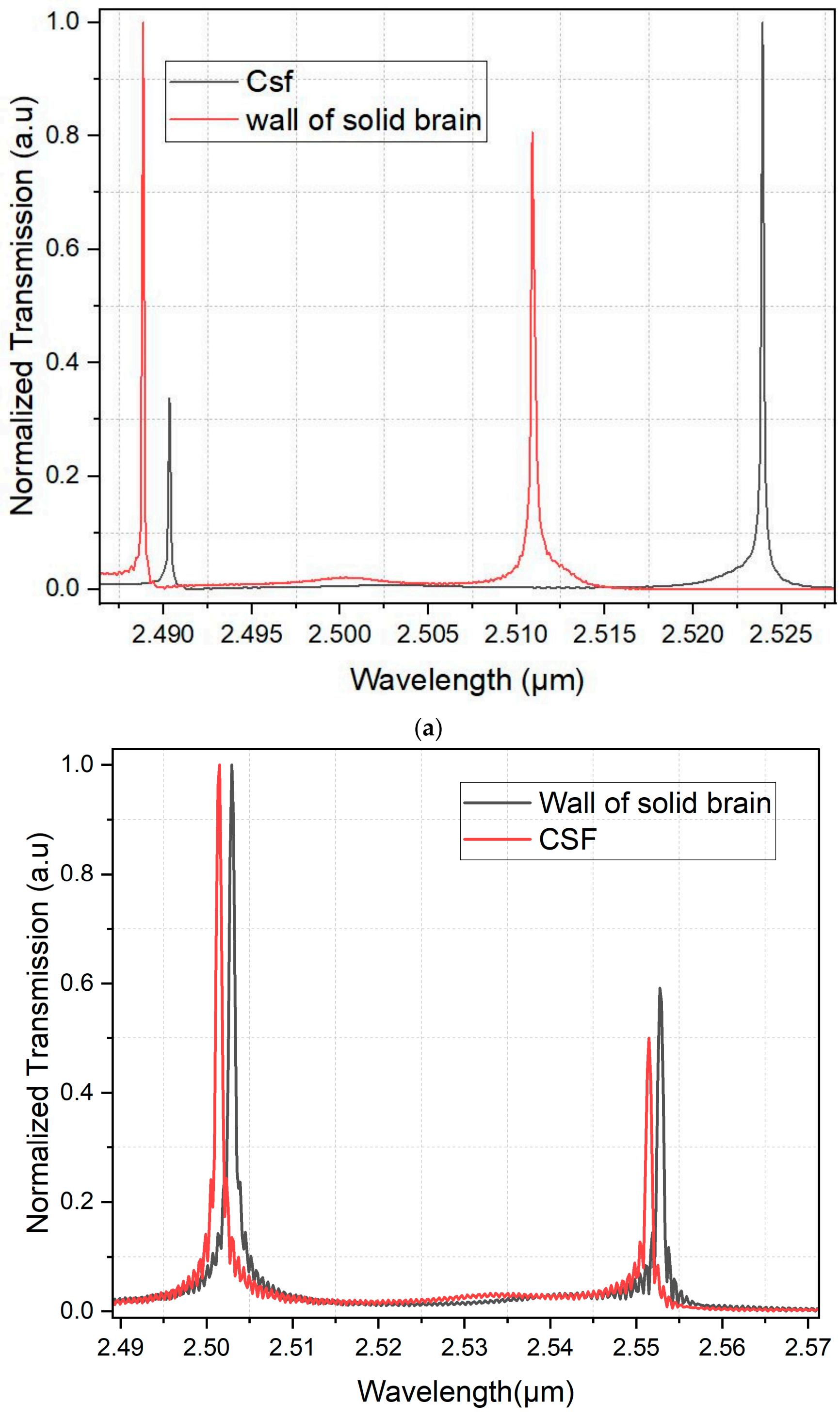

(**a**)

(**b**)

Figure 5. Output normalized transmission (**a**) Detection with dual-cavity configuration, (**b**) detection with single-cavity configuration.

Q-factor signifies that the resonator stores energy for a longer time before it is lost and it is given by:

$$Q = \frac{\omega_0}{FWHM} \tag{2}$$

where

- ω_0 is the resonant angular frequency.
- $FWHM$ is the full-width at half-maximum of the resonance spectrum.

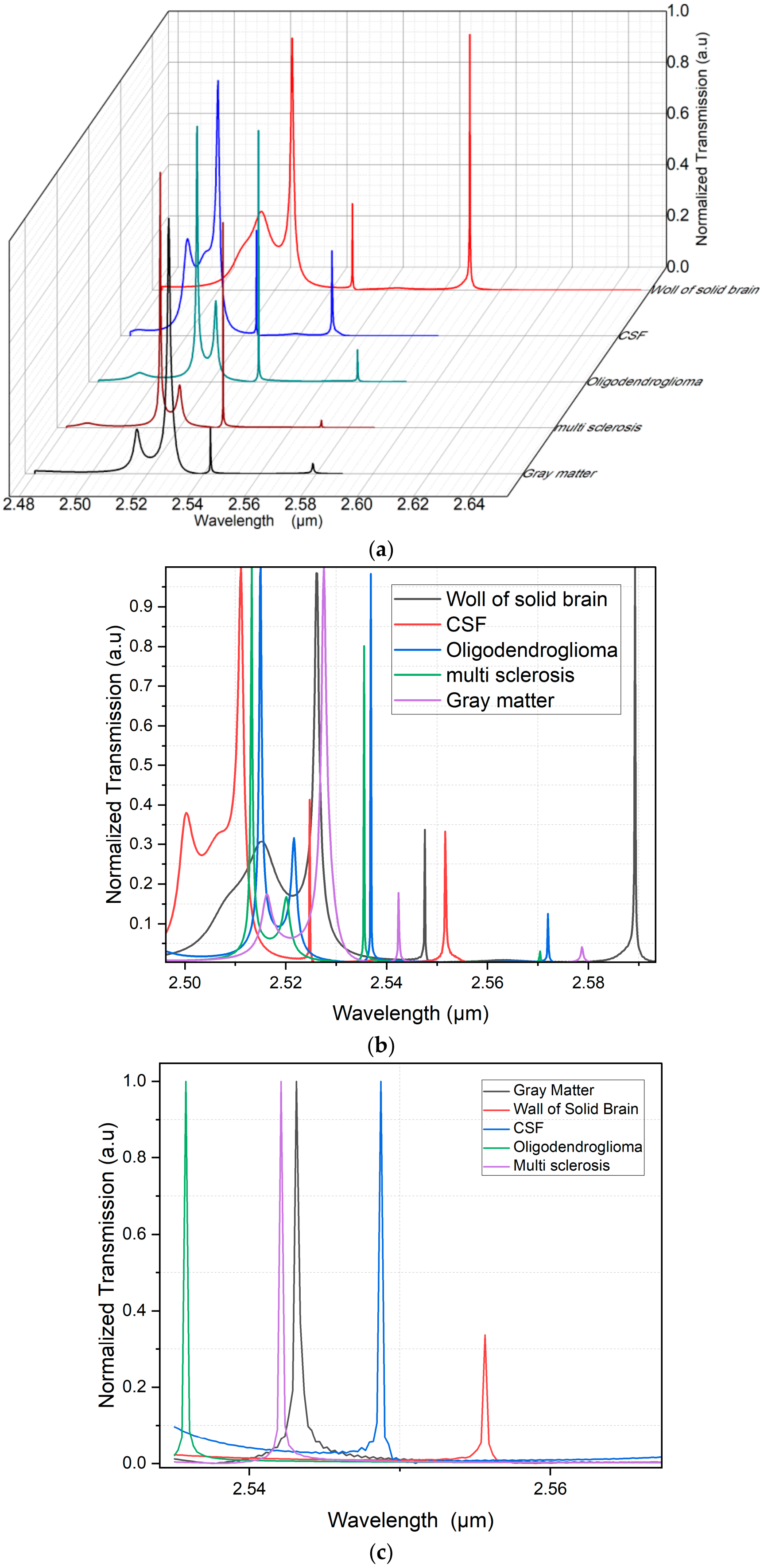

(**a**)

(**b**)

(**c**)

Figure 6. Normal brain cells detection (**a**) 3D visualization, (**b**) 2D visualization, (**c**) best sharp mode shift.

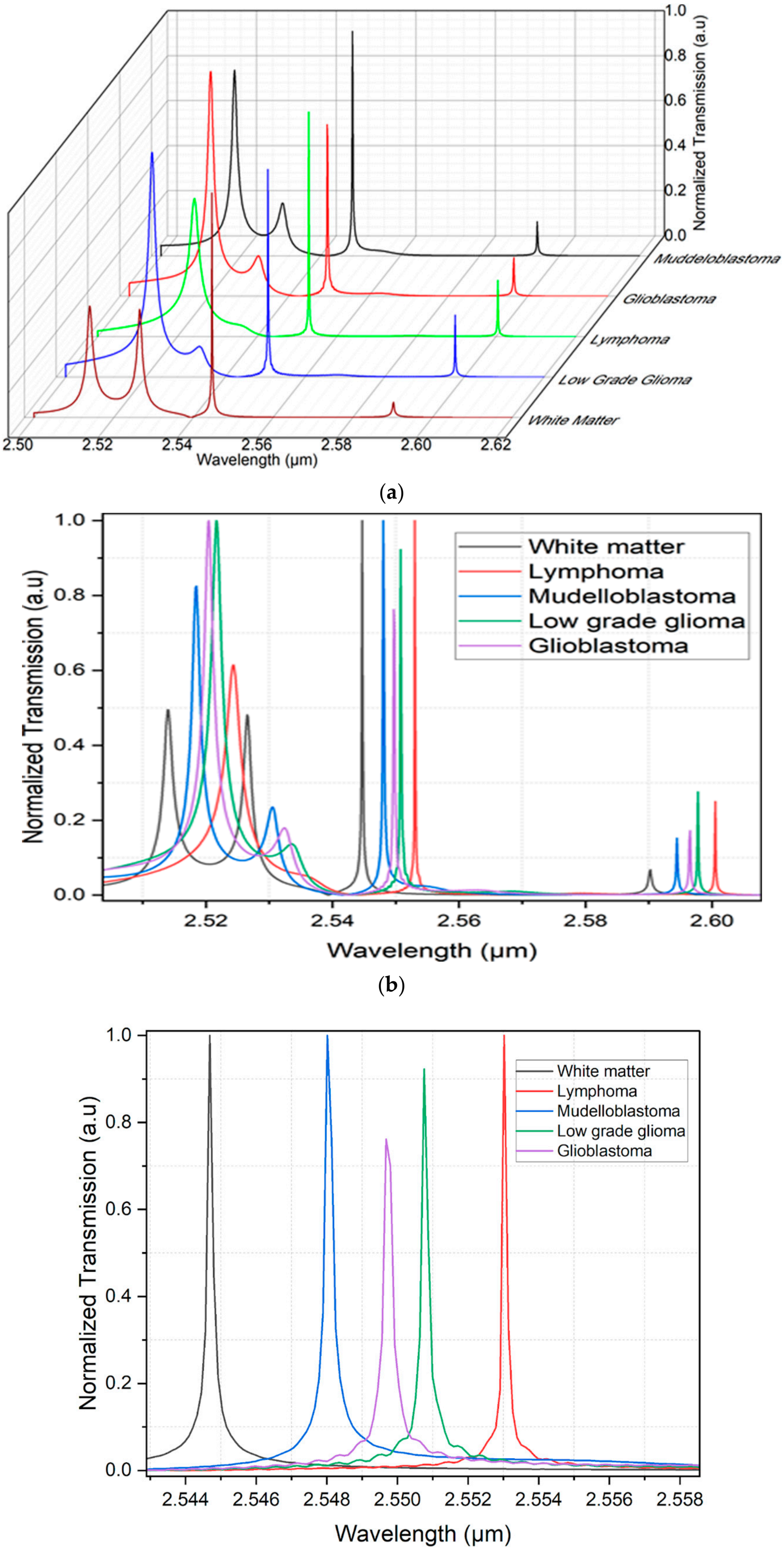

(**a**)

(**b**)

(**c**)

Figure 7. Malignant brain cells detection (**a**) 3D visualization, (**b**) 2D visualization, (**c**) best sharp mode shift.

The second mode presents a sharp Gaussian profile with high intensity, indicating a high quality factor and strong electromagnetic field confinement. In contrast, the third mode exhibits a sharp peak with lower intensity, suggesting a moderate Q-factor and weaker confinement. Owing to its superior field localization and higher intensity, the second mode is selected for detailed analysis and is illustrated in Figure 6c.

Although a single H0-type cavity ideally supports a fundamental defect mode, the proposed structure is coupled to photonic crystal waveguides. This coupling, together with symmetry perturbations and finite-size effects, can excite higher-order and waveguide-assisted resonant modes, resulting in multiple observable resonance peaks within the photonic bandgap.

The most significant resonance modes observed in the transmission spectra are analyzed separately to provide a detailed understanding of their characteristics. The corresponding results are summarized in Table 2, including the central resonant wavelength, peak intensity, full width at half maximum (*FWHM*), sensitivity, quality factor, and figure of merit (*FOM*), which quantifies the sensor's sensitivity relative to the resonance linewidth. It is defined by:

$$FOM = \frac{S}{FWHM} \tag{3}$$

and the detection limit which defines the smallest refractive index change n that the sensor can reliably detect. It is given by:

$$DL = \frac{\Delta\lambda_{min}}{S} \tag{4}$$

Table 2. Photonic crystal sensor parameters for normal and malignant brain cells obtained using the dual-cavity two-dimensional photonic crystal configuration, including refractive index (RI), resonant modes, central wavelength, full width at half maximum (*FWHM*), quality factor (Q), sensitivity (*S*), figure of merit (*FOM*), and detection limit (*DL*).

Tissue	RI	Mode	Center	Height	FWHM	Q	S	FOM	DL
					Normal Cells				
CSF	1.3333	1	2.51	0.71	0.00163	1540.50	1912.66	1,173,409.96	8.8×10^{-7}
		2	2.52	0.41	0.00017	14,463.37	2888.61	16,547,840.55	5.8×10^{-7}
Wall of Brain	1.3412	1	2.53	0.75	0.00152	1661.92	9915.38	6,523,279.35	1.7×10^{-7}
		2	2.55	0.34	0.00021	12,392.24	9261.54	45,051,433.10	1.8×10^{-7}
Multisclerosis	1.3425	1	2.51	0.78	0.00072	3503.70	1954.10	2,724,217.38	8.6×10^{-7}
		2	2.54	0.80	0.00018	14,265.65	416.54	2,343,587.82	4.0×10^{-6}
Oligodendroglioma	1.3353	1	2.53	0.87	0.00421	600.30	132.97	31,583.23	1.26×10^{-5}
Gray Matter	1.3951	1	2.52	0.49	0.00266	947.12	504.26	189,573.28	3.33×10^{-6}
		2	2.56	0.73	0.00033	7857.68	970.19	2,980,897.42	1.73×10^{-6}
					Malignant Cells				
White Matter	1.4121	1	2.51	0.37	0.00289	869.92	1538.19	532,246.01	1.09×10^{-6}
		2	2.54	0.95	0.00021	12,026.51	2855.43	13,495,131.07	5.9×10^{-7}
Low-Grade Glioma	1.432	1	2.52	0.75	0.00317	795.47	2872.83	906,254.29	5.8×10^{-7}
Medulloblastoma	1.4412	1	2.52	0.61	0.00197	1278.39	339.66	172,413.79	4.95×10^{-6}
		2	2.55	0.92	0.00034	7590.45	289.66	862,857.35	5.8×10^{-6}
Glioblastoma	1.447	1	2.52	0.75	0.00349	722.17	307.44	88,091.12	5.46×10^{-6}
		2	2.55	0.74	0.00033	7647.32	272.73	817,978.96	6.16×10^{-6}
Lymphoma	1.4591	1	2.52	0.46	0.00580	435.19	–	–	–
		2	2.55	0.99	0.00017	15,352.38	–	–	–

It should be noted that Lymphoma corresponds to the highest refractive index value investigated in this work. As a result, no further analyte is available to define a resonance wavelength shift relative to Lymphoma. Consequently, sensitivity-related parameters such as sensitivity, figure of merit, and detection limit cannot be evaluated for this case and are therefore omitted from Table 2.

In normal tissues, high Q-factors appear in Mode 2 across multiple normal tissues (e.g., CSF Mode 2: 14,463.37, Wall of Brain Mode 2: 12,392.24), suggesting narrow, stable resonances. Normal tissues like Wall of Brain and Multisclerosis show very high sensitivity in both modes (Wall of Brain: 9915.38 and 9261.54). Their low detection limits (e.g., 1.7×10^{-7} RIU for Wall of Brain) make them excellent reference or baselines for sensing.

Malignant tissues show lower or moderate Q-factors in Mode 1 (e.g., glioblastoma: 722.17). But in some cases, there was an extremely high Q in Mode 2 (e.g., lymphoma: 15,352.38), indicating a strong and sharp resonance.

Sensitivity is relatively lower in most malignant cases compared to normal tissues. Glaucoma and Lymphoma show low sensitivity in Mode 2 (272–307 nm/RIU), indicating less responsive modes.

The results of the photonic crystal sensor show that normal brain tissues have sharp and consistent resonance peaks with high *FOM* values (often ≈ 1 million), indicating strong signal quality and low loss. Malignant tissues, in contrast, exhibit broader and more variable peaks with lower *FOMs*, reflecting higher damping. Mode 2 provides better precision due to higher Q-factors and lower detection limits, while Mode 1 offers stronger, more visible peaks, useful for rapid or visual detection. These differences support the sensor's effectiveness in distinguishing between healthy and cancerous tissues.

The results obtained from the photonic crystal sensor developed in this study demonstrate significant advancements in the detection of brain cancer subtypes. Compared to similar designs reported in the literature, the proposed structure exhibits superior performance across several key metrics. The sensor achieves exceptionally high sensitivity values, reaching up to 9915.38 nm/RIU, with quality factors (Q-factors) exceeding 15,000 in certain resonant modes, values that are rarely achieved in standard photonic crystal biosensors, which typically report Q-factors in the range of 500 to 10,000.

Furthermore, the figure of merit (FOM), which combines sensitivity and resonance sharpness, reaches values as high as 4.5×10^{7}, indicating the sensor's exceptional ability to distinguish subtle refractive index variations. The detection limit (DL), a critical parameter for clinical applications, is as low as 1.7×10^{-7} RIU, surpassing the common detection thresholds observed in similar optical biosensors.

Notably, this sensor operates in a dual-mode detection regime, enabling the analysis of multiple resonance peaks per tissue type, which enhances measurement reliability and specificity. The design successfully differentiates between various brain tissues and cancer types, including glioblastoma, medulloblastoma, lymphoma, and low-grade glioma, offering high precision in cancer subtype identification.

To further clarify the origin of the observed performance enhancement in the dual-cavity configuration, the underlying physical mechanism is discussed below.

6. Physical Mechanism of Dual-Cavity Enhancement

The enhanced sensing performance observed in the dual-cavity configuration can be attributed to the coupled-resonator effect arising from the interaction between two adjacent photonic crystal cavities. When two cavities are placed in close proximity, evanescent coupling occurs, leading to the formation of hybrid supermodes with stronger electromagnetic field confinement within the cavity region. This coupling effectively increases the photon lifetime, as light is stored for a longer duration due to multiple reflections and energy exchange between the cavities, resulting in a significantly higher quality factor (Q-factor).

Moreover, the dual-cavity configuration enhances field localization in the sensing region, producing higher optical energy density where the analyte is present. This increased spatial confinement strengthens the interaction between the resonant optical mode and the infiltrated cerebrospinal fluid, thereby enhancing the sensor's sensitivity to refractive index variations. Consequently, even minute variations in the refractive index induce larger resonance wavelength shifts compared to the single-cavity case. This coupled-resonator mechanism directly explains the observed enhancement in sensing performance, including the increase in sensitivity up to 9261.54 nm/RIU, the improvement of the quality factor beyond 15,000, and the reduction in the detection limit to the order of 10^{-7} RIU.

It should be emphasized that increasing the number of coupled cavities does not necessarily lead to monotonically improved sensing performance. In coupled-resonator photonic crystal systems, adding more cavities introduces additional resonant modes and stronger mode splitting, which can increase inter-mode interference and radiation losses. These effects may broaden the resonance linewidth and degrade the quality factor, ultimately limiting further sensitivity enhancement. From a practical fabrication perspective, increasing the number of coupled cavities requires tighter control over cavity spacing, geometry, and alignment tolerances, making the device more sensitive to fabrication imperfections. Similar non-monotonic behavior has been reported in previous studies on coupled-cavity photonic crystal sensors [2,15].

7. Comparison with Recent Dual-Cavity Photonic Crystal Biosensors

The comparison is restricted to photonic crystal sensors employing dual- or double-cavity architectures to ensure a fair and structurally consistent performance evaluation.

As shown in Table 3, the proposed dual-cavity photonic crystal sensor outperforms previously reported dual-cavity designs in terms of sensitivity and detection limit, while maintaining a high quality factor.

Table 3. Comparison of recently reported dual-cavity photonic crystal sensors.

Ref.	Sensor Structure	Sensitivity (nm/RIU)	Q-Factor	DL
[2]	2D Dual-cavity PhC biosensor	79	–	–
[18]	2D Double nanohole cavity PhC	217.66	6151.58	4×10^{-3}
This work	2D Dual-cavity PhC sensor	9261.54	15,352.38	$<1.7 \times 10^{-7}$

8. Conclusions

A brain cancer sensor based on a two-dimensional photonic crystal coupler has been numerically investigated using the OptiFDTD software (Version 12.1). The proposed design was analyzed under single- and dual-cavity configurations to evaluate the effect of cavity number on sensing performance. The results demonstrate that doubling the number of cavities while maintaining identical structural parameters significantly enhances the sensor characteristics. In particular, the dual-cavity configuration achieves a high sensitivity of 9261.54 nm/RIU, a quality factor of 15,352.38, and a detection limit below 1.7×10^{-7} RIU, indicating a substantial improvement compared to the single-cavity design. These enhancements originate from stronger cavity–waveguide coupling and improved electromagnetic field confinement, which result in sharper resonance features and increased light–matter interaction. Overall, the proposed dual-cavity photonic crystal sensor shows strong potential for high-precision refractive index sensing in biomedical applications, particularly for early brain cancer detection.

Author Contributions: Conceptualization, S.B.; methodology, S.B. and N.D.; software, S.B. and N.D.; validation, S.B. and N.D.; formal analysis, S.B. and N.D.; investigation, S.B.; resources, A.H., A.Y. and

O.S.; data curation, S.B.; writing—original draft preparation, S.B. and N.D.; visualization, S.B. and N.D.; supervision, N.D. and A.H.; project administration, A.H., A.Y. and O.S. All authors have read and agreed to the published version of the manuscript.

Funding: This research received no external funding.

Data Availability Statement: The original contributions presented in this study are included in the article. Further inquiries can be directed to the corresponding author.

Conflicts of Interest: The authors declare no conflict of interest.

References

1. Malek, C.; Al-Dossari, M.; Awasthi, S.K.; Matar, Z.S.; El-Gawaad, N.S.A.; Sabra, W.; Aly, A.H. Employing the Defective Photonic Crystal Composed of Nanocomposite Superconducting Material in Detection of Cancerous Brain Tumors Biosensor: Computational Study. *Crystals* **2022**, *12*, 540. [CrossRef]
2. Zhang, Y.-N.; Zhao, Y.; Lv, R.-Q. A review for optical sensors based on photonic crystal cavities. *Sens. Actuators A Phys.* **2015**, *233*, 374–389. [CrossRef]
3. Yang, D.-Q.; Duan, B.; Liu, X.; Wang, A.-Q.; Li, X.-G.; Ji, Y.-F. Photonic Crystal Nanobeam Cavities for Nanoscale Optical Sensing: A Review. *Micromachines* **2020**, *11*, 72. [CrossRef] [PubMed]
4. Djeffal, N.; Bendib, S.; Hedir, A. A Dengue Virus Detection Using Biosensor-Based Two-Dimensional Photonic Crystal Ring Resonator. *Photonics* **2025**, *12*, 514. [CrossRef]
5. Bendib, S.; Zegadi, A.; Djeffal, N. Improved sensitivity of 2D annular photonic crystal biosensor working at THz frequency range. *Opt. Quantum Electron.* **2016**, *48*, 528. [CrossRef]
6. Bendib, S.; Bendib, C. Biosensors & Bioelectronics Photonic Crystals for Malaria Detection. *J. Biosens. Bioelectron.* **2018**, *9*, 3. [CrossRef]
7. Su, D.; Pu, S.; Mao, L.; Wang, Z.; Qian, K. A photonic crystal magnetic field sensor using a shoulder-coupled resonant cavity infiltrated with magnetic fluid. *Sensors* **2016**, *16*, 2157. [CrossRef] [PubMed]
8. Pu, S.; Bai, X.; Wang, L. Temperature dependence of photonic crystals based on thermoresponsive magnetic fluids. *J. Magn. Magn. Mater.* **2011**, *323*, 2866–2871. [CrossRef]
9. Yu, G.; Pu, S.; Wang, X.; Ji, H. Tunable one-dimensional photonic crystals based on magnetic fluids. *Opt. Int. J. Light Electron Opt.* **2013**, *124*, 2713–2715. [CrossRef]
10. Pu, S.; Liu, M. Tunable photonic crystals based on $MnFe_2O_4$ magnetic fluids by magnetic fields. *J. Alloys Compd.* **2009**, *481*, 851–854. [CrossRef]
11. Nouman, W.M.; Abd El-Ghany, S.E.S.; Sallam, S.M.; Dawood, A.F.B.; Aly, A.H. Biophotonic sensor for rapid detection of brain lesions using 1D photonic crystal. *Opt. Quantum Electron.* **2020**, *52*, 287. [CrossRef]
12. Maher, M.A.; Aly, A.H.; Esmail, M.S.; El-Ghany, S.E.S.A. Maximizing temperature sensitivity in a one-dimensional photonic crystal thermal sensor. *Sci. Rep.* **2025**, *15*, 4105. [CrossRef] [PubMed]
13. Mohammed, N.A.; Khedr, O.E.; El-Rabaie, E.S.M.; Khalaf, A.A.M. Brain tumors biomedical sensor with high-quality factor and ultra-compact size based on nanocavity 2D photonic crystal. *Alex. Eng. J.* **2023**, *64*, 527–540. [CrossRef]
14. S, S.B.; Bahaddur, I. Rapid Detection of Brain Lesions using Biosensor Based 2D Photonic Crystal. In Proceedings of the 2021 IEEE International Conference on Electronics, Computing and Communication Technologies (CONECCT), Bangalore, India, 9–11 July 2021; pp. 1–6. [CrossRef]
15. Boulesbaa, M.; Mekimah, B.; Guermache, A. Design and analysis of 2D photonic crystals biosensor based on a dual-cavity for brain tissue detection. *Optik* **2025**, *322*, 172160. [CrossRef]
16. Sakka, L.; Coll, G.; Chazal, J. Anatomy and physiology of cerebrospinal fluid. *Eur. Ann. Otorhinolaryngol. Head Neck Dis.* **2011**, *128*, 309–316. [CrossRef] [PubMed]
17. Wright, B.L.C.; Lai, J.T.F.; Sinclair, A.J. Cerebrospinal fluid and lumbar puncture: A practical review. *J. Neurol.* **2012**, *259*, 1530–1545. [CrossRef] [PubMed]
18. Gowdhami, D.; Balaji, V.R. Analysis and design of photonic crystal malaria biosensor with double nanohole cavity resonator with ultra-high-quality factor. *Opt. Quant. Electron.* **2024**, *56*, 593. [CrossRef]